A SANS and APT study of precipitate evolution and strengthening in a maraging steel

T.H. Simm, L. Sun, D.R. Galvin, D. Alba Venero, Y. Li, T.L. Martin, P.A.J. Bagot, M.P. Moody, P. Hill, H.K.D.H. Bhadeshia, S. Birosca, M.J. Rawson, K.M. Perkins

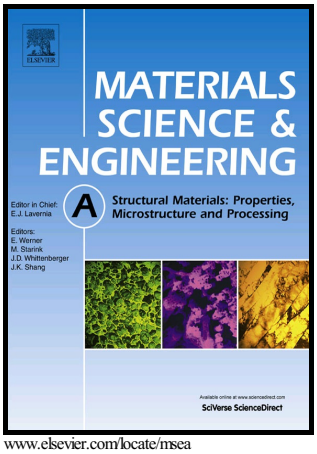

www.elsevier.com/locate/msea

PII: S0921-5093(17)30908-5
DOI: http://dx.doi.org/10.1016/j.msea.2017.07.013
Reference: MSA35261

To appear in: *Materials Science & Engineering A*

Received date: 6 May 2017
Revised date: 6 July 2017
Accepted date: 7 July 2017

Cite this article as: T.H. Simm, L. Sun, D.R. Galvin, D. Alba Venero, Y. Li, T.L. Martin, P.A.J. Bagot, M.P. Moody, P. Hill, H.K.D.H. Bhadeshia, S. Birosca, M.J. Rawson and K.M. Perkins, A SANS and APT study of precipitate evolution and strengthening in a maraging steel, *Materials Science & Engineering A,* http://dx.doi.org/10.1016/j.msea.2017.07.013

A SANS and APT study of precipitate evolution and strengthening in a maraging steel

T.H. Simm[a*], L. Sun[b], D.R. Galvin[a], D. Alba Venero[e], Y. Li[a], T.L. Martin[d], P.A.J. Bagot[d], M.P. Moody[d], P. Hill[c], H.K.D.H. Bhadeshia[b], S. Birosca[a], M.J. Rawson[c], K.M. Perkins[a]
[a]*Swansea University, SA1 8EN, UK.*
[b]*University of Cambridge, Cambridge, CB3 0FS, UK.*
[c]*Rolls-Royce plc, Derby, UK,*
[d]*University of Oxford, Oxford, OX1 3PH, UK,*
[e]ISIS Facility, STFC, Didcot, OX11 0QX.
[*]T.H.Simm@Swansea.ac.uk /
Thomas.Simm@dMata.co.uk.

Abstract

In this work a combination of the characterisation techniques small angle neutron scattering (SANS) and atom probe tomography (APT) are used to study the precipitation in a maraging steel. Three similar maraging steel alloys were aged at different temperatures and ageing times, and then characterised using SANS, APT and microhardness. The alloys consist of two types of precipitates, namely Laves phase and β-NiAl, the precipitates have different composition and hence precipitate ageing, which makes it complicated to model. The SANS experimental set-up was relatively simple and allowed the precipitate size and fraction of a large number of samples to be measured in a single experiment. The APT results were used for constraining the SANS modelling, particularly the composition, shape and distribution of phases. The characterisation led to the following description of precipitation: NiAl phase reaches coarsening at early stages of ageing and shifts its strength mechanisms from shearing to Orowan looping, which cause the characteristic peak strength; the Laves phase is in growth throughout and its strength contribution increases with ageing time. These observations were shown to be consistent with precipitate evolution and strengthening

models, and the work of others. Although, there are some issues with the combination of SANS and APT approach, which are discussed, the methodology provides a valuable tool to understand complex precipitation behaviours.

Keywords: small angle neutron scattering (SANS); atom probe tomography (APT); Steel; Precipitation strengthening; NiAl; Laves phase

1 Introduction

Maraging steels are a class of steel used within the aerospace sector because of their ultra-high strength, combined with good fatigue and toughness properties [1,2]. These alloys gain their beneficial properties by a fine dispersion of a nano-scale precipitates, produced after an ageing heat-treatment at an elevated temperature. To understand the mechanical properties, and optimise thermo-mechanical processing routes, it is important to be able to understand this ageing and how the precipitates influence the mechanical performance. It is over 100 years since the discovery of precipitation strengthening [3] and around 70 years since a theory of the mechanisms causing this strengthening was developed [4]. Since then there have been numerous studies on precipitation strengthening and theories on the mechanisms involved [3,5–9]. There has been some success in modelling the precipitation strengthening, but there is still a general uncertainty about the exact approach to take for a given alloy. This is particularly the case for steel alloys or when the precipitates are small (e.g. less than ~10 nm), and it is not obvious what model to use or the values of the parameters within these equations. The issue is further complicated because of the difficulty in quantifying the precipitates present. Because of this it is common to take a two-step approach; in the first step the precipitation growth kinetics are modelled to provide information of the

precipitate population, and in the second step the strengthening is calculated from the predicted precipitate population. This two-step approach is not ideal because both processes are difficult to model, but is used mainly due to the difficulty in quantifying the precipitate population. For example, it may be possible to predict the final strength from the heat-treatment applied, without the models predicting either the precipitate evolution or the strengthening.

Quantifying the precipitate population in a sample is difficult. Transmission electron microscopy (TEM) is the most widely used characterisation technique, but there are limitations with this method including: how characteristic of the bulk is the small volume measured, an uncertainty quantifying precipitate size and density, and even observing the precipitates themselves when they are small, coherent with the matrix or have similar chemistry to the matrix. This latter case is not uncommon, especially for precipitates at the earliest stages of ageing; such as for some common precipitates in steels such as NiAl and α'_{Cr}. Atom probe tomography (APT) has proved itself to be a useful technique to quantify these small and coherent precipitates [1,10–12]. However, the volume sampled is smaller even than TEM, and so its use on its own should be treated with care and in most cases it is not feasible to use APT to do bulk analysis. When the precipitates are large or more heterogeneously distributed, there can be problems with both APT and TEM techniques because of the small size sampled. In this case SEM using the back-scattered mode can be effective. Small angle scattering (SAS) is a bulk analysis diffraction technique that can be used to gain quantifiable information about the size and volume fraction of nano-sized precipitates. The technique has been used for metals [13–18], but is more commonly used within other areas of science. For example, it is well used in colloidal science where in the ideal case precipitates are

diluted, nearly monodispersed and the matrix is generally homogeneous [19]. Its use within metals has been limited perhaps because of the increased complexity of metallic systems; because there are many length-scales involved and even the matrix is not homogeneous. Like any technique the analysis of SANS and APT data is dependent on the hypothesis and approximations (or assumptions) used, and we will try to explain why we made the assumptions we did and the possible influence that these assumptions have on the results.

The aim of this paper is to quantify the precipitations through APT and SANS. Although challenging, and not widely used, we think that relevant information could be extracted if a careful and critical analysis of the results is done. We will do this for a novel maraging steel with three major phases; a BCC martensitic matrix, with NiAl and Laves phase precipitates. The experimental data will be used to verify models for the evolution and strengthening of precipitates.

2 Materials and Methods

The composition of the alloys studied are shown in Table 1. The alloys were produced by Allvac Ltd by vacuum induction melting- vacuum arc remelting (VIM-VAR) and subsequently homogenised and forged. Samples were austenised at temperatures between 900 °C and 960 °C, in the fully austenite region for each alloy, to ensure precipitation only occurs during ageing. They were then cooled to produce a fully martensitic microstructure. The samples were then aged at temperatures between 520 °C and 560 °C for several hours. Hardness measurements were made with a load of 30 kg using a Vickers microhardness machine from polished samples. From heat-treated samples, specimens were prepared for TEM, APT and SANS measurements.

Table 1 the chemical composition of the maraging steels, and the composition of precipitates, in atomic %.

	Al	*Co*	*Cr*	*Fe*	*Mo*	*Ni*	*W*
LowAl	**2.56**	**7.96**	**10.91**	**69.35**	**1.62**	**6.85**	**0.75**
9922	**3.58**	**7.91**	**9.72**	**68.31**	**1.17**	**8.71**	**0.60**
F1E	**3.66**	**7.95**	**10.74**	**68.49**	**1.62**	**6.80**	**0.75**

Thin foil transmission electron microscopy (TEM) specimens were mechanically thinned and then electropolished. TEM thin foils were examined using a Philips CM30 TEM with a LaB_6 source operating at 300 kV. For APT matchsticks of 0.5 mm × 0.5 mm × 20 mm were machined and subsequently electropolished into needle-shaped specimens. All APT specimens were analysed using a Cameca LEAP 3000X HR atom probe, in pulsed-laser mode using a 532 nm wavelength laser, operated at 0.4 nJ and 200 kHz using a base specimen temperature of 50 K. Reconstruction and analysis was performed using the commercial software IVAS version 3.6.6. SANS measurements were carried out at the Quokka beamline, ANSTO, Australia. The wavevector transfer (or scattering vector q) was measured over a range of values from 0.003 $Å^{-1}$ to 0.74 $Å^{-1}$, which was achieved from three different sample to detector distances of 1.3 m, 12 m and 20 m. The scattering vector is given by $q = 4\pi.sin\theta/\lambda$, where λ, is the wavelength and 2θ is the angle between incident and scattered beams. This configuration allowed us to maximize the accessible q-range. Since the wavevector transfer is a reciprocal distance unit, the lower q will probe longer correlation lengths, while the high-q end will probe the shorter ones. The wavelength used was 5 Å, with a 10% spread ($\Delta\lambda / \lambda = 0.1$), and the source and sample aperture diameters were 50 mm

and 5 mm. SANS data was reduced using the Igor software package and transformed to absolute scale by the use of an attenuated direct beam transmission measurement.

3 Analysis Procedure

3.1 Atom Probe Tomography

Size values were obtained by creating isosurfaces (regions where the composition of an element is above a certain composition) around the precipitates of 17% Ni and 7% Mo (in atm.%) for NiAl and Laves phase respectively (more details can be found in [20]). These values were chosen as they were half-way between the maximum concentration within a precipitate and the matrix composition. This choice is somewhat arbitrary, and will influence the size values obtained (lower values will give bigger precipitates). However, the values were chosen based on the isosurface maps to produce precipitates that did not significantly overlap or were unrealistically small. These isosurfaces were used to create a list of precipitates, with their own volume and position. Average equivalent circular diameter (ECD) size values were obtained from the list, by taking the arithmetic mean and by fitting the size values to a log normal distribution.

A proximity histogram (or proxigram) provides the concentration profile as a function of distance either side of the interface defined by an isosurface [21]. The compositions of the precipitates were determined from these composition proxigrams using the values at the centre of the precipitates: for Laves phase the value used was when the composition is almost constant, and for NiAl when it has reached a maximum value within the precipitate. We have taken account of the cross-over of the 27 Da peak (an overlap in the APT mass/charge state ratio spectra between $^{54}Fe^{2+}$ and $^{27}Al^{+}$ ion isotopes [11]) by assuming that within the matrix and Laves phase this peak corresponds entirely to Fe and inside NiAl it corresponds entirely to Al. Matrix compositions were calculated

by creating isosurfaces of Ni and Mo with concentration levels lower than used for calculating precipitate size and taking the matrix as the composition outside this region. Volume fractions were calculated in two ways from APT: (1) by the number of atoms within an isosurface, the Atom count approach, (2) or by the composition of phases, the Lever rule approach. In the atom count approach, the fraction of atoms within each phase (using the isosurfaces determined for size quantification) gives the volume fraction. There will be a slight uncertainty here because of different mass densities of the precipitates, which was ignored. The lever rule method is normally used for binary systems; in the method, the fraction of a phase can be found by comparing the composition of the total system (i.e. before ageing) with the composition of the two phases (i.e. after ageing). In a system with three phases the treatment is more complicated, and was solved by using a fitting algorithm. In this the fraction of the phases are fitting parameters which reduce the difference between the composition of phases calculated using the Lever rule and those measured. In the fitting the elements were limited to: Mo, Fe, W, Ni...

3.2 Small Angle Neutron Scattering

The small angle neutron scattering cross section is defined as [22]:

$$\frac{\partial \Sigma(q)}{\partial \Omega} = NV^2(\Delta\rho)^2 P(q)S(q) + Bcg \qquad (1)$$

where *N* is the number of precipitates per unit volume, each with volume *V*. The function *P(q)* is the scatterer form factor (it is related with the Fourier transform of the shape of the individual scatterers) and *S(q)* the structure factor. *S(q)* is a measure of the interparticle structural correlations, and tends to 1 [22] for dilute systems; for simplicity we have assumed a dilute system and it can be ignored. $\Delta\rho$ is the difference in scattering length density between precipitate and matrix, where ρ is given by:

$$\rho = \frac{n_a}{V_a}\sum_i x_i\, b_i \qquad (2)$$

where n_a and V_a are the number of atoms and volume of the unit cell respectively, x_i is the composition of element i in atomic fraction and b_i the elements neutron scattering length [23]. As can be seen in eq. 1, the SANS intensity varies with the square of the difference of the SLDs of the matrix and the scatterer, and linearly with the volume fraction. So for example, doubling the volume fraction and reducing $\Delta\rho$ by a factor of 4 will have no influence at all in the scattering curve.

The scattered intensity ($I(q)$) was fitted to the following function [24,25]:

$$I(q) = \frac{\varphi_\beta}{V_\beta}\left[\frac{3V_\beta\Delta\rho_\beta\left(\sin qr_\beta - qr_\beta\cos qr_\beta\right)}{\left(qr_\beta\right)^3}\right]^2 + \frac{\varphi_L}{V_L}\left[\frac{3V_L\Delta\rho_L(\sin qr'_L - qr'_L\cos qr)}{(qr'_L)^3}\right]^2$$

$$+ GP(q) + Bcg$$

$$r'_L = [R_b^2\sin^2\alpha + R_a^2\cos^2\alpha]^{1/2} \qquad (3)$$

where φ is the volume fraction of the phase, given by the subscript β for NiAl and L for Laves; r is the radius of the precipitate, r' the equivalent radius of an ellipsoid found from the angle α between the axis of the ellipsoid and the q-vector and the radius along the rotational axis R_a and perpendicular to this R_b; V is the volume of the sphere/ellipsoid, $GP(q)$ is the Guinier Porod function and is used to model the scattering from the martensitic matrix [25]; and Bcg is the instrument background. The functions were chosen based on the different shapes of the precipitates, with NiAl close to a sphere, and Laves phase closer to an ellipsoid. The least-square fitting of the curve was carried out using SasView.

Example fits of the data are shown in Figure **1**. Before ageing (0 h) the intensity increases considerably at low values of q and is well described by a Guinier Porod function; since no precipitates are present this is probably indicative of considerable

scattering from the martensite. One of our main working hypothesis is that the scattering of the matrix does not change with the heat treatment. It is known that the microstructure of the matrix will change, but the evolution of the different nano-precipitates is much faster. Therefore, we have used the 0 h scan to represent the matrix contribution to the total scattering signal at all other ageing times. After 12.5 h ageing, two 'bumps' develop in the scattering pattern. The position of these bumps gives an indication of the size of the precipitate (see Eq. 3), with lower q-values corresponding to larger precipitates. Hence, the bump at low q (~$2x10^{-2}$ $Å^{-1}$) stems from the Laves phase and the high q bump (~$7x10^{-2}$ $Å^{-1}$) from NiAl; such that the precipitates are separated based only on their size. We believe this is a good approximation as TEM and APT measurements show that NiAl precipitates are smaller than Laves phase at all ageing times measured. At shorter ageing times, when the size of both precipitates is similar, it would be difficult to separate the contributions of both phases.

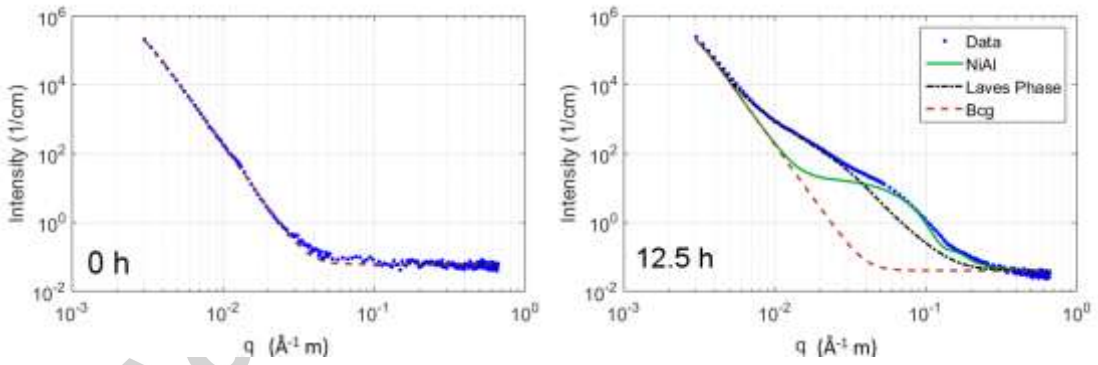

Figure 1, example SANS fit of 9922 aged at 540 °C for 12.5 h, showing the Guinier Porod plus background scattering from the matrix (brown dashed line), NiAl (green full line), Laves phase (black dot-dashed line) and the experimental data (blue dots).

During fitting we assume that the scattering from the matrix and background are constant (whilst there is some change in the background level between samples it does not change in a systematic way) and only allow φ_β * and φ_L* to vary during fitting (*

refers to the fact that these are nominal values which will be adjusted). When using the composition values found from APT the volume fraction values obtained using equation 3 were unrealistically high, particularly for NiAl. This is addressed in the Supplement along with possible reasons for the discrepancy. To correct for this, we multiplied the volume fractions of each precipitate by a constant factor so that they matched the volume fraction values obtained by APT at a particular ageing time.

There will be compositional changes, of both the matrix and precipitates, happening during the ageing process. The change in the composition of the precipitates is relatively small (discussed in the following section) but the change of the matrix will be larger. Since the composition of precipitate and matrix directly relates to the volume fraction these changes will influence the volume fraction values. An approach to account for this is discussed in the Supplement. This approach leads to a correction to the volume fraction values relative to an assumption of a constant composition of matrix and precipitate. This correction is relatively small in the case studied, but this need not be the case in all situations. Due to the uncertainty in determining the absolute values of the volume fraction of the phases and the correction for a changing matrix being relatively small, it is assumed that both the matrix and precipitate composition are constant across all ageing times and temperatures. A comparison of the volume fractions found by APT and SANS for the alloys is provided in the results section.

A constant size distribution was assumed with *PD* ratios (*PD*= standard deviation / mean) of 0.5 for Laves phase and 0.3 for NiAl, based on values found from APT and TEM results.

The final approximation we make is to reduce the inherent random errors involved in SANS. In this correction, we average the size and volume fraction values from three

different alloys. The justification for this step is that the relative differences between the size and volume fractions of the different alloys are smaller than the uncertainty in the results of a particular alloy. The sizes of the different alloy types are an average of the three melts, and the volume fraction of Laves and NiAl phases in the different alloy types are also an average, but with a different magnitude for each phase and melt. These corrections are discussed in more detail in Supplement along with individual fits to the different alloys datasets.

4 Results

4.1 Precipitation

Two techniques were combined with the SANS analysis to understand the precipitation in this alloy: transmission electron microscopy (TEM) and atom probe microscopy (APT). The information from these techniques is then fed into the SANS models. In Figure 2 are TEM micrographs of alloy 9922 after austenisation and ageing. Figure 2a shows the microstructure after only an austenisation heat-treatment. No precipitates can be observed in the micrographs after the austenisation process. This was also observed in the other melts and is consistent with previous work [12]. After ageing two types of precipitates start to form, (1) Laves phase which have an irregular shape and often form on lath or other grain boundaries, (2) NiAl phase which is smaller, more evenly distributed and approximately spherical. NiAl are difficult to quantify by TEM because of their small size and poor contrast (due to their coherency with the matrix). APT was used to gain more information on both phases, and in particular NiAl. In Figure 3 are isosurface maps of Ni and Mo used to indicate NiAl and Laves phase, respectively. From the figure, after 7.5 h ageing it is apparent that the two types of precipitates are markedly different. NiAl are a few nanometres in size, approximately spherical and

spread evenly through the matrix; whereas, Laves phase are larger (about 10 times larger than NiAl), with a lower number density and a more irregular shape. At 0.5 h this distinction in size is less apparent but the precipitate density and shape differences are still observed. In Figure 4, are comparisons of the composition proxigrams of two different alloy types (9922 and lowAl) and two different ageing times (0.5 h and 7.5 h for 9922). There is considerable overlap of the composition profiles of the two precipitates for different alloy type and ageing times. This observation is the justification for the assumption that the composition of NiAl and Laves phase are constant across all ageing times and alloys studied.

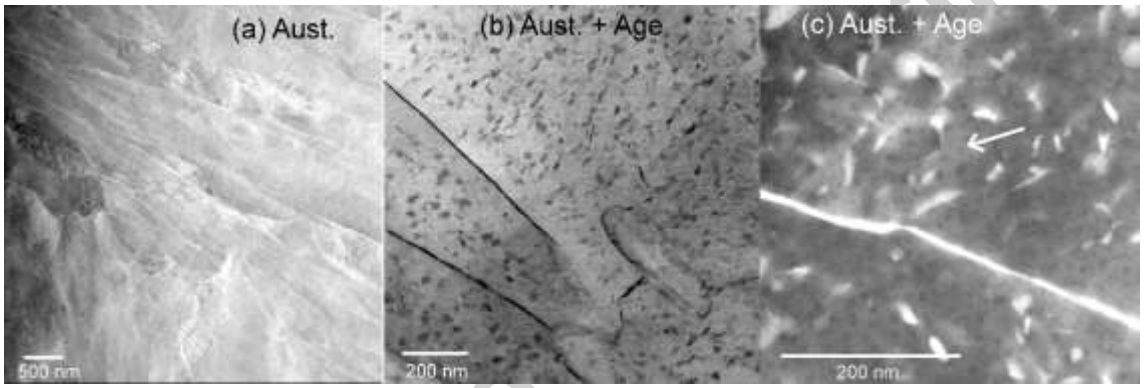

Figure 2, TEM micrographs of alloy type 9922, after austenisation only (a), and austenisation and then aged at 540 °C for 10 h (b, c). The darker particles in b and the lighter particles in c are Laves phase. The arrow in c indicates a region where NiAl phase are visible as darker particles. (a) and (b) are bright-field images and (c) a dark-field image.

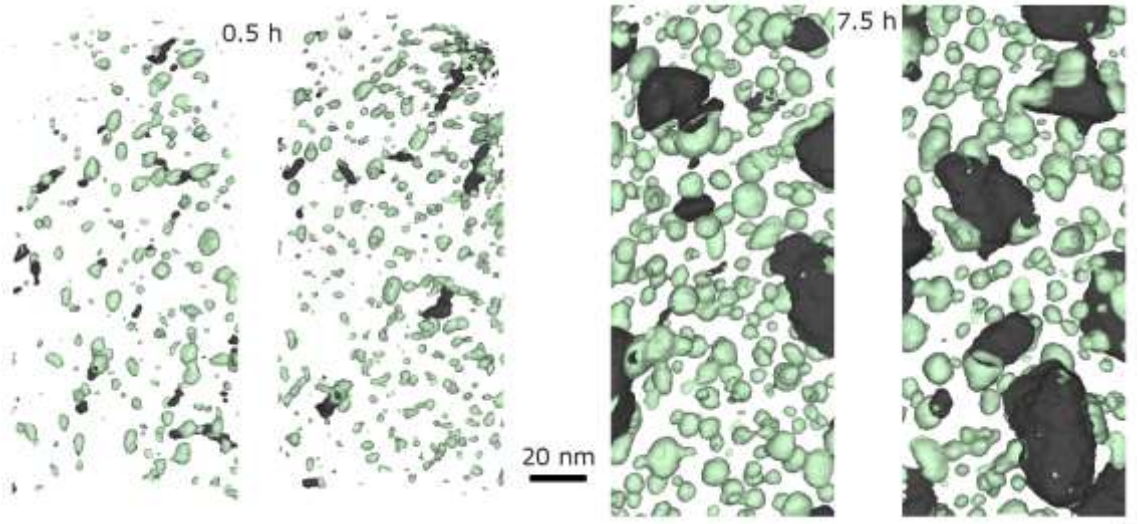

Figure 3, APT isosurfaces of 9922 after austenisation and ageing at 540 °C. Showing isosurfaces of Ni (17 atm.%) in green to represent NiAl and Mo (7 atm.%) in black to represent Laves phase. On the left are the precipitates after ageing for 0.5 h, and on the right after ageing for 7.5 h. The regions are rectangular 20 nm in depth, 80 nm in width and ~160 nm in height.

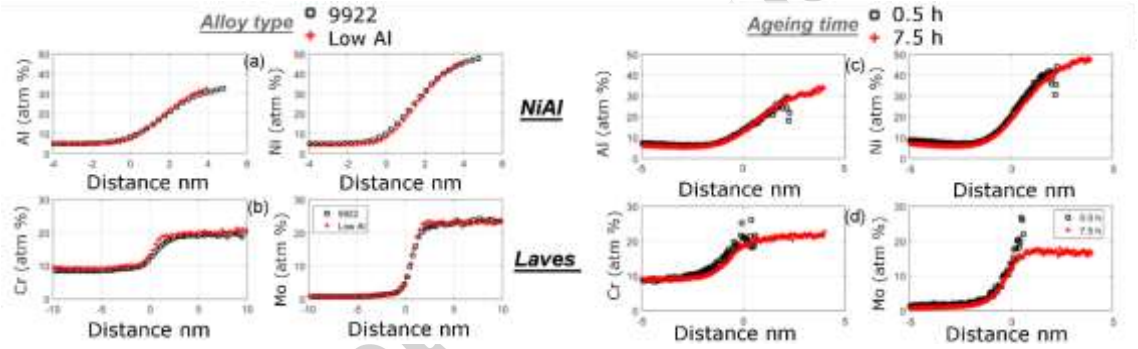

Figure 4, composition proxigrams for the 9922 alloy for the NiAl (a and c) and for laves phase (b and d) for selected elements, Al and Ni for NiAl, and Cr and Mo for laves phase. (a) and (b) show the difference in alloy chemistry and (c) and (d) the difference in ageing time.

4.2 Precipitate Evolution

The change in the volume fraction and sizes of the precipitates for alloy 9922 derived by SANS analysis are shown in Figure 5. The evolution in the volume fraction of the two precipitates is markedly different. For Laves phase it increases with ageing time at all temperatures; whereas for NiAl the value increases rapidly before saturation, such

that for the times measured (>1 h) it is approximately constant. There are differences in the changes in volume fraction with temperature; for Laves phase the volume fraction increases more quickly with increased temperature, whereas for NiAl the volume fractions are slightly higher at lower temperatures. For both NiAl and Laves phase the size increases with ageing time and temperature following a power law relationship (details of this are discussed later). The increase in size with ageing time is approximately linear on this logarithm plot, with a similar gradient for both precipitates but the Laves phase are ~7 times larger.

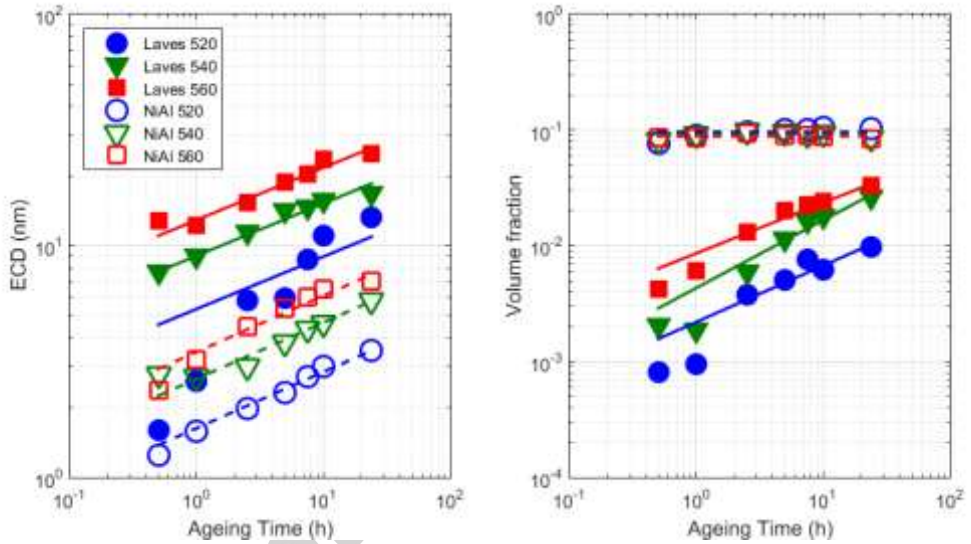

Figure 5, the change in the equivalent crystal diameter *(ECD)* and volume fraction (φ) with ageing time of the averaged data. The lines are fits to the average data using Eq. 7 for ECD values with one value of n_3 for Laves phase and one for NiAl. The volume fraction values for the Laves phase are fits to Eq. 4.

4.3 Precipitate Strengthening

Ageing to produce a distribution of small precipitates is crucial for obtaining the beneficial mechanical properties of this alloy. For example, the Vickers hardness increases by almost two times after ageing. Different ageing times and temperatures produce different precipitate populations (i.e. sizes, volume fractions and distributions)

and so it would be expected that this would lead to different mechanical properties. This is indeed the case as shown in Figure 6, the hardness changes with ageing time and temperature. There are some notable features of these results: (1) the strength at each temperature increases to a maximum and then falls, (2) the ageing time needed to reach this maximum, i.e. the peak-hardness, increases as the ageing temperature falls, and (3) the peak-hardness strength increases as the ageing temperature decreases.

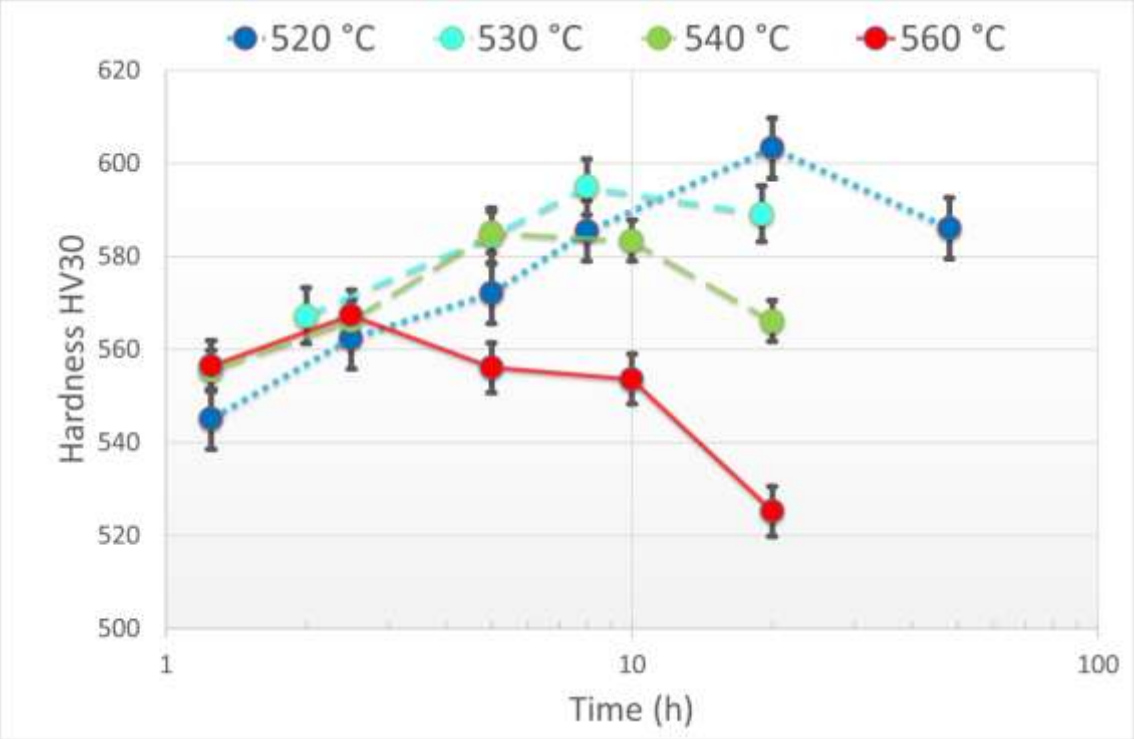

Figure 6, the change in Vickers hardness of 9922 with ageing time and temperature. The error bars represent the standard deviation in the measurements.

5 Discussion

5.1 Precipitate Evolution

The typical evolution of a precipitate during ageing can be separated into three stages: (1) initiation, (2) growth and (3) coarsening; although in practical situations there will be some crossover between these [26]. The difference between these stages is shown schematically in Figure 7. In the nucleation stage, small regions of elevated solute

concentration, close to the equilibrium of the precipitate, are formed throughout the matrix. Because of their small size the volume fraction during the nucleation stage is relatively small compared to the equilibrium volume fraction. In the growth stage the volume fraction increases to a maximum value as the precipitates grow. During the coarsening stage the volume fraction remains approximately constant but the average size continues to increase as larger precipitates grow at the expense of smaller precipitates. The results of Figure 4 suggest that NiAl is in the coarsening stage from ~1 h onwards, because the volume fraction is approximately constant after this time. In contrast, Laves phase is in the growth stage for all temperatures and times, as evidenced by the increases in volume fraction with time at all temperatures.

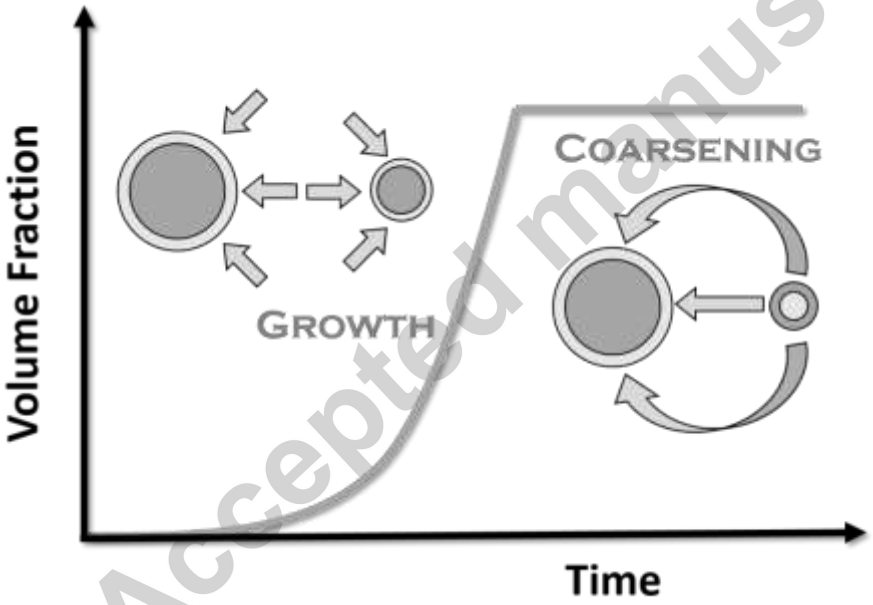

Figure 7, schematic of the stages of evolution of a precipitate. Where, in the nucleation stage the precipitate number increases dramatically but the volume fraction stays relatively small. This is followed by the growth stage where the volume fraction increases to a maximum. In the final stage, coarsening, the volume fraction stays approximately constant but the number of precipitates falls.

The change in the volume fraction of a precipitate (φ) with time, t, during the growth stage can be given by the following formulae [27], where f_T is the fraction of a phase transformed:

$$f_T = 1 - exp\left(-\frac{\pi}{3} N_r G_r^3 t^{n_f}\right),\ f_T \to k_f t^{n_f}\ as\ t \to 0,\ k_f = \frac{\pi}{3} N_r G_r^3 \quad (4)$$

where, N_r and G_r are constants related to the nucleation and growth rates, respectively, of the precipitate. Both variables are proportional to the speed of this diffusion or diffusivity (D), along with other parameters. The diffusivity is temperature dependent and can be given by the following formulae [27]:

$$D = D_0 \exp\left(-\frac{Q_0}{RT}\right),\ \text{where}\ D_0 = \sum_i x'_i D_i^0\ \text{and}\ Q_0 = \sum_i x'_i Q_i^0 \quad (5)$$

Where, D_0 and Q_0 are diffusivity constants that are used to determine the diffusivity D of an element at different temperatures. R is the universal gas constant and x'_i is the volume fraction of element i. The diffusivities of different elements present in the alloy are shown in Table 2; the elements with the highest diffusivities are Ni and Al, and the lowest is Cr followed by Co and Mo [26,28–30]. Using the compositions of the precipitates and Eq. 5 the diffusivity of NiAl is found to be at least 15 times higher than Laves phase. This large difference may explain why from the SANS results, the two precipitate types appear to be in different stages of evolution, and why the Laves phase reaches the end of the growth stage at least more than 20 times slower than NiAl. The results are also in general agreement with the work of other researchers on Laves phase and NiAl [31–34].

It is possible to assess the change in the volume fraction of Laves phase by plotting $ln(-ln(1-f_T))$ against $ln(t)$: n_f is found from the gradient of the plot and k_f from the intercept. The value of n_f has been measured and calculated to have a range of values from 1 to

over 2.5. If an assumption is made that the mean composition of the matrix decays exponentially with time, the value of n_f has been shown to be close to unity [5,35–37]. A closer approximation to observed precipitation kinetics is described by the Johnson-Mehl-Avrami (JMA) equation, which leads to a range of possible n_f values: (a) if there is no nucleation within the growth stage $n_f = 1.5$, (b) and if nucleation occurs with an increasing rate during growth $n_f > 2.5$. Experimental work on alloys with similar Laves phase precipitates [33,38] have found n_f values between 1.3 and 1.6, which are consistent with the predictions based on separate nucleation and growth stages. In this work, using SANS and APT, n_f is found to be around 1 (Table 3 and Supplement). The values are of the same order as the predicted values (particularly when using the values found from fitting to the alloys separately); however, the values are lower by around one third than other results and predictions and may suggest a limitation of the theoretical approach or a different mechanism at play (e.g. a shift to coarsening).

The volume fractions that we obtained from the SANS analysis, using the composition values of precipitates and matrix from APT, were unrealistically high, particularly for NiAl (discussed in Supplement 1). Hence, the values of each phase was multiplied by a constant (effectively creating a new SLD for each precipitate) to match the APT data at a particular ageing time and temperature (540 °C for 7.5 h). The cause of this discrepancy is not clear, but is thought to be due to the difficulty in obtaining composition of small precipitates by APT and additional scattering between the two phases which was ignored. The normalised SANS volume fraction values are the ones discussed in this report. An important issue that this raises is that it is easier to obtain relative volume fraction changes than absolute values when using SANS. The composition of a precipitate can change significantly with the composition of an alloy

and the ageing temperature [12], and because of the difficulty in obtaining the composition of precipitates, there will always be an uncertainty when obtaining absolute volume fraction values.

The volume fractions of NiAl and Laves phase measured by APT are shown in Table 4. Since the two APT approaches use different features of the microstructure the results are expected to differ, but are in most cases very close. From previous work [12] it was shown that the standard deviation in the volume fraction of an APT specimen was considerable. This is also expected to be the case here since only one specimen was measured per condition. The volume fraction of Laves phase is very low at 0.5 h, and increases more rapidly than NiAl between 0.5 h to 7.5 h: by 2-4 times for NiAl in contrast with 20-29 time for Laves phase.

The composition values found by APT and SANS are consistent with each other, both in terms of the differences between the alloys and between the two ageing times. Further investigation would be needed at intermediate ageing times to compare details of the precipitate evolution, such as when NiAl reaches coarsening or the rates of increase. However, the changes in the volume fraction of Laves phase with ageing time as measured by SANS (particularly from n_f), discussed above, give some justification that the changes in volume fraction by SANS are reasonable.

Table 2, diffusivities taken from the literature. Ref-A at 550 °C [28]**, Ref-B at 510 °C** [30]**, Ref-C** [29] **at 550 °C and 475 °C. Ref-D** [26] **is used with the other references for the calculated range of values shown.**

		NiAl	*Laves*	*Al*	*Co*	*Cr*	*Fe*	*Mo*	*Ni*	*W*
Literatur e	**D (x 10^{-22}**			**93,000 [A]**	31 [B]	5.0 [A] and 160	230 [A]	20 and 600 [C]),	360 [A] and 56	
Calculated	**D at 540 °C**	**24 13,000**	**to 0.00083 to 870**	**$5.9x10^4$ to**	1.5 to 130	0.00045 to 3.2	0.39 to 150	5.0×10^{-12} to 240	1.9 to 230	2.8×10^{-25} to 3.2
	D_0 (x 10^{-4})	**1.8 110**	**to 4.1 to 4.4**							
	Q_0 (x 10^5)	**2.5 to 2.6**	**2.4 to 3.4**							

It is possible to use the obtained sizes of the precipitates to extract information about the precipitate evolution. Theoretically the precipitate radius (r) increases with the aging time (t) following [37]:

$$r^{n_3} - r_0^{n_3} = ct \qquad \text{with } c = \frac{c'D}{T} = \frac{c'}{T} D_0 \exp\left(-\frac{Q_0}{RT}\right) \tag{7}$$

where, r_0 is the initial size of the precipitate (equal to 0 during growth, or for coarsening equal to the precipitate size at the beginning of the coarsening behaviour), c and n_3 are constants related to the nature of the growth of the precipitate. The value of c is proportional to the diffusivity D of the precipitate and related to the temperature, along with other variables [37].

The values of the constants in Eq. 7 were determined from fitting the equation to the SANS size results, and are shown in Table 3, Q_0 relates the ageing temperature, at an ageing time, to the corresponding size of a precipitate (i.e. a bigger value of Q_0 corresponds to a wider spacing in sizes at different temperatures). The value of Q_0 is similar for the two precipitates (4.1×10^5 for NiAl and 4.9×10^5 for Laves phase) but slightly higher for Laves phase. In Table 2, we have made a calculation of Q_0 for the two precipitates based on the composition of the elements within them (2.5×10^5 and

2.9 x 10^5). The calculated values are lower than those obtained by SANS, but are of the same order: ~0.6 of the SANS values (more details are provided in the Supplement). This difference in Q_0 means that the spread in sizes at different temperatures is larger in the SANS results than expected by the calculated values. The cause of the difference is not clear; it could be due to the uncertainty in calculating the Q_0 from diffusivity data or due to the assumptions made in the SANS analysis. However, the SANS results do show the value of Q_0 to be higher in Laves phase than NiAl by 20%, which is consistent with the 16% calculated.

The constant n_3 indicates how the size changes with time (whereas Q_0 indicates how it changes with temperature). From theory n_3 can have a range of values. From classical derivations the value of n_3 can be shown to be equal to 2 for particle growth [39] and 3 for coarsening. The value will also be higher if precipitation occurs on a boundary instead of the matrix, e.g. during coarsening the value of n_3 increases from 3 to 4 if precipitation occurs on the grain boundary rather than by lattice diffusion [40]. Figure 5 shows that the power law behaviour of equation 7 is met for the size data. For NiAl the value of n_3 is ~3.9 for all temperatures and is therefore ~25% higher than the theoretical value of 3. For Laves phase the value of n_3 is found to be ~3.1, slightly smaller than that found for NiAl. The value of n_3 for Laves phase is ~1/3 higher than the theoretical value of 2. The discrepancy may be due to limitations of the model since it is based on spherical precipitates and lattice diffusion [39], or because Laves phase favours formation on boundaries.

Table 3, values of n_f (see Equation 4), n_3 and Q_0 (see Equation 7) found from fitting the SANS data. * See supplement for more details on the difference.

	NiAl	Laves
$\mathbf{n_f}$	-	*0.90 / 1.16**
$\mathbf{n_3}$	*3.93*	*3.07*
$\mathbf{Q_0}$	*4.14 x 10^5*	*4.89 x 10^5*

Table 4, volume fraction values obtained from APT, by atom count and lever rule methods, and from SANS.

Alloy	Time (h)	NiAl			Laves		
		Atom Count	Lever Rule	SANS	Atom Count	Lever Rule	SANS
LowAl	7.5	7.4%	5.9%	5.8%	2.7%	1.5%	3.3%
9922	0.5	7.9%	1.6%	-	0.13%	0.09%	-
9922	7.5	15%	7.0%	9.2%	2.6%	2.6%	1.5%
F1E	7.5	7.0%	6.7%	8.0%	4.1%	2.3%	2.6%

Frequency histograms of size values from APT measurements of 9922 at the two ageing times are shown in Figure 8, and the average size values by both APT and SANS are shown in Table 5. The histogram and table show a general agreement with the SANS results. The NiAl precipitates are smaller and more frequent than Laves phase (the maximum frequency value is approximately 20x higher for NiAl) at both ageing times, and the size of both phases increases with ageing time. There is an overlap in the size distributions of the precipitate sizes, which is expected from the SANS analysis. However, the difference in sizes found by APT at 0.5 h is much smaller than the difference found by SANS. As previously mentioned before, it is difficult to separate the contribution from both phases at the early stages of the ageing due to their similar size. There is also a difference in the absolute values obtained. This is probably due to several factors. One factor that may explain the results is that the atom density, obtained by APT, within both precipitates is lower than the matrix. It is thought that this is an artefact from the measurement, i.e. the density is constant. If this is the case then it

would cause the precipitates to appear bigger than they are and could explain the differences.

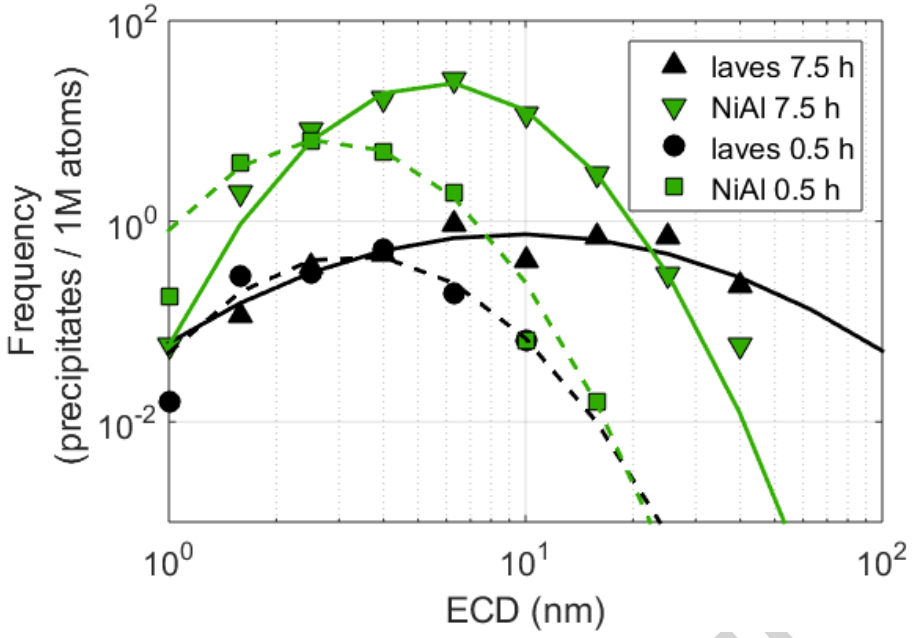

Figure 8, ECD size frequency histograms for NiAl and Laves phase after 0.5 h and 7.5 h ageing at 540 °C of 9922, determined by APT. The lines represent fits of the data to a lognormal distribution.

Table 5, ECD size values determined by SANS and APT analysis of 9922 after ageing for 0.5 h and 7.5 h at 540 °C. APT log is the mean size from the fit of the size values to a lognormal distribution and APT mean is the mean of the size values.

	NiAl ECD Size (nm)			Laves ECD Size (nm)		
	APT log	**APT mean**	**SANS**	**APT log**	**APT mean**	**SANS**
9922: 0.5 h	*4.0*	*3.2*	*2.3*	*5.3*	*3.8*	*7.7*
9922: 7.5 h	*8.3*	*6.4*	*4.3*	*44.7*	*13.5*	*14.3*

5.2 Precipitate Strengthening

There are several different models that can be used to relate the precipitate distribution to an alloy's strength. The most well-known of these was developed by Orowan [4], and describes the strengthening from the looping of dislocations between hard undeformable particles. Although, the same general form of the equation is used by most researchers,

the exact relationship between strength and precipitate population (volume fraction and size) can differ as different relations are used. A large part of this is due to the difficulty in defining the interparticle spacing, *L*, from volume fraction and precipitate size values. When the precipitates are small (less than ~ 10 nm *ECD*) the dislocations can cut through the particles. In this case the strengthening can be shown to be due to a number of factors [3,41–43] (more detail is provided in the Supplement). As with the Orowan formulae these relations can be slightly different and lead to different strength results for the same precipitate population. In addition, the formulae can contain values that are difficult to determine, such as the lattice misfit between precipitate and matrix [44].

When using the SANS data with the strengthening formulae, we find that different Orowan or shearing formulae give different magnitudes but have similar overall behaviour (Figure 9). For example, the Orowan strengthening can change by a factor of ~10 depending on the formulation used (or ~ 2 for the two formulae used in Figure 9b), mainly because of how the distribution is defined. But in all cases the different Orowan formulae cause the value of laves strengthening to increase in a similar manner, and NiAl strengthening to fall in a similar manner. When precipitates are sheared by dislocation a number of formulae have been determined to describe the strengthening, including chemical, stacking-fault, modulus, order and coherency strengthening [5,41]. In Figure 9a some of these formulae have been used to determine the shear strengthening of NiAl and laves precipitates using the SANS data. In contrast, the shear strength increases with ageing time for both precipitates, in a similar manner to the change in strength of laves phase for the Orowan mechanism. The shear dispersion formula is not shown here for NiAl but falls in a similar manner to the Orowan curves. Since this equation is intended for use when the precipitate size is larger [45], it offers a

different explanation to the change in mechanism than the shear to Orowan mechanism proposed in the text. The large variations in the magnitude and the different behaviours of the two strengthening mechanisms means that many points (i.e. ageing times with different volume fractions and sizes) are required to understand the relative strengthening contributions.

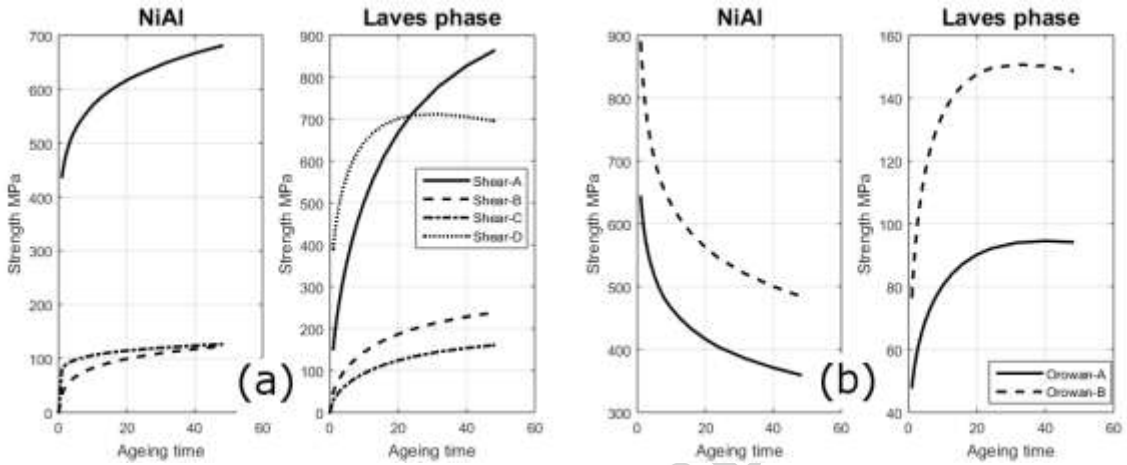

Figure 9, the strengthening of precipitates using different shear strengthening formulae (a). And the strengthening by different Orowan strength formulae (b). Both strengthening predictions use the SANS data of 9922 at 540 °C. Shear-A Friedel formula from [46] **and used in [10]. Shear-B chemical strengthening, Shear-C coherency strengthening, Shear-D dispersion strengthening** [45]**. Orowan-A** [47] **and Orowan-B uses the Orowan equation in Eq. 10.**

To model strengthening we use an Orowan equation [43] for Laves phase, because of their larger size across all ageing conditions. Although at low ageing times this approximation may become less valid, any potential error is reduced because of the lower volume fractions. For the NiAl phase we consider the strengthening from both Orowan looping and shearing [43,46], where the active mechanism is the one that offers the least resistance to dislocation movement. The approach works is in a similar manner to the one described by Schnitzer and colleagues [48], whereby strengthening is given by a shearing mechanism below a critical particle size and an Orowan mechanism above

this. The approach is used here because no individual strengthening equation can describe the characteristic peak-hardness. An equation for the strengthening from a fine distribution of precipitates developed by Ansell and Lenel [49], could partly explain the peak-hardness. However, given that the model is only dependent on the volume fraction of the precipitates it fails to explain the differences at different ageing temperatures. The following equations are used for precipitate strengthening:

$$\Delta\sigma_{Oro} = \frac{0.81 M_T G b \ln\frac{2r_s}{b}}{4\pi r_s\left[\left(\frac{\pi}{4\varphi}\right)^{\frac{1}{2}}-1\right](1-\nu)^{\frac{1}{2}}}, where\ r_s = \left(\frac{2}{3}\right)^{\frac{1}{2}} r \quad (8)$$

$$\Delta\sigma_{\beta} = min\left(\Omega_{\beta,Oro} \middle| \kappa_{\beta ratio}\Omega_{\beta,Sh}\right)$$

$$\Delta\sigma_{\beta,Oro} = (\varphi)^{\frac{1}{2}}\frac{0.81 M_T G b \ln\frac{2r_s}{b}}{4\pi r_s\left[\left(\frac{\pi}{4}\right)^{\frac{1}{2}}-0.2\right](1-\nu)^{\frac{1}{2}}}\ \Delta\sigma_{\beta,Sh} = (\varphi)^{\frac{1}{2}}\frac{2M_T S}{br(\pi\omega_q)^{\frac{1}{2}}}\left(\frac{\gamma\omega_r r}{S}\right)^{\frac{3}{2}} \quad (9)$$

where, M_T is the Taylor factor, G the shear modulus of the matrix, b the magnitude of the Burgers vector of dislocations, ν the Poissons ratio, $\omega_{q,r}$ constants derived from particle statistics, S is the dislocation line tension given by $S=Gb^2/2$, r the particle radius and φ the volume fraction. For NiAl we also assume there is a normal distribution of particle sizes (st. dev. = 1 nm), and the total strengthening is the sum of the contributions. This has the effect of smoothing the transition between the two mechanisms (Figure 10a).

In addition to precipitation strengthening, the alloy will also gain strength from the lath structure (subscript *l*), due to the intrinsic strength of iron (*Fe*), and solid solution strengthening (*SS*). As with many other strengthening mechanisms, the one produced by solid solution strengthening is not well defined. Different relationships between the composition (χ) of solute elements and strengthening are found by different researchers, with both different values of the exponent of the composition (either 1 or 1.5 are

commonly used) and proportionality constants [50–53]. The strengthening can also change in a complex way with an increase in the percentage of the element (such as increasing and then decreasing [51]). Based on the strength of the alloy before ageing (see Supplement) we define the strength from these contributions by the following formulae:

$\Delta\sigma_{SS}(HV) = 14.5x'_{Al} + 14.5x'_{Mo} - 4.5x'_{Ni} + 14.5x'_{W}\ \ HV$, where x' is in weight %

$$\sigma_0 = \sigma_{Fe} + \sigma_l = 260.5\ HV \quad (10)$$

Due to the issues highlighted above with different strengthening equations, we use a semi-empirical approach to determine the strengthening during ageing. We will use the SANS data and formulae (Equations 8, 9 and 10) that relate the volume fraction and size of precipitates to strengthening. To quantify the contribution of each different mechanism we will fit the hardness values to the following equation:

$$\sigma_Y = \sigma_0 + \Delta\sigma_{SS} + \kappa_L\Delta\sigma_{Oro} + \kappa_\beta\Delta\sigma_\beta \quad (11)$$

κ_L, κ_β and $\kappa_{\beta ratio}$ are fitting variables and the other parameters are found from Eq. 8 to 10. We are using different fitting variables for Orowan strengthening of NiAl and Laves phase because the distribution of precipitates is different and this will lead to different values of *L*. In all, three fitting variables are used.

In Figure 10, the results of the semi-empirical strengthening model for 9922 are shown. In Figure 10a, the predicted strengthening of NiAl is shown, along with the strengthening by Orowan and shear mechanisms. The strengthening by Orowan falls with increasing ageing times and increases as the temperature is lowered. The jump in Orowan strengthening at the start of ageing is caused by the rapid increase in the volume fraction of NiAl determined from SANS measurements. The relative behaviour of Orowan and shear strengthening means that the minimum of the two mechanism

provides the characteristic shape of the hardness curves: a steep increase in strength to a maximum followed by a gradual fall in strength, with maxima that increases in time with falling temperature. In contrast, the Orowan strengthening of Laves phase increases with time in a similar way to NiAl shear strengthening (Figure 10a). The behaviour of Laves strengthening, with ageing temperature, is more complicated because there are large changes in both the size and the volume fraction. Consequently, smaller precipitates with a smaller volume fraction (lower temperatures) have a similar strengthening to larger precipitates with a greater volume fraction. The solid solution (SS) strengthening falls with ageing time as more strengthening elements diffuse into Laves phase. Because the volume fraction of Laves phase increases quicker at higher temperatures the SS strengthening is lower at higher temperatures. A notable feature of the predicted NiAl strengthening is that the strength maxima are approximately constant with ageing temperature. Therefore, in order to explain the increase in the peak strength with falling temperature the increase in Laves phase strengthening must be larger than the fall in SS strengthening. The strength predictions show that NiAl and intrinsic strengthening (SS, lath and Fe strengthening) dominate at low ageing times, whereas Laves phase only becomes the dominant precipitate strengthening mechanism after long ageing times (>50 h). Figure 10b, displays the measured (which have been interpolated) and predicted strength values. The predictions show many of the features of the measured values, including the positions and magnitudes of the peak strengths and strength values that are close to those predicted. But there are some discrepancies with the predictions, (1) the time to peak strength are further spread out than the actual data (i.e. the predicted time to peak strength is too low at 560 °C and too high at 520 °C), and (2) a more gradual rise in strength at 520 °C than found. This analysis suggests that

the model can explain features of the age hardening of the alloy but not the complete behaviour. This is to be expected given that the method is simple and there is a good probability of at least some errors in the SANS results because of this. A more detailed approach would be to establish the exact nature of the Orowan, shear and solid solution models (and relationships to volume fraction and size) by isolating one phase at a time. For example, a possible explanation for the discrepancy at low ageing times at 520 °C may be caused by small Laves phase contributing to strength by a shear mechanism.

The formulism used here leads to the same conclusion as Schnitzer and colleagues [48] of a critical precipitate size in which particles change mechanism from shearing to Orowan looping. The value we obtain for 9922 is ~4.4 nm, and changes by less than 0.1 nm for the different temperatures. This is lower than the value they obtained of 13.6 nm, however the difference may be due to their limited data particularly before peak hardness.

The three parameters found when fitting Eq. 12 to the hardness values of 9922, were then used for the other two alloys. The predicted strengthening of all three alloys, along with the difference in volume fraction of precipitates, are shown in Figure 11. Because of the formulation used, the time to peak strength is the same for all alloys as is the shape of the contributions. The magnitude of the different strengthening contributions varies significantly between the alloys, because of the differences in volume fraction of the precipitates in the different alloys (Figure 11). The predicted and measured strength values show some agreement, i.e. F1E has the maximum strength and the other two have similar and lower strengths and the time to peak-strength, which appears to be approximately constant for this set of alloys (see also Supplement). The difference between predictions and measurements is larger for F1E. Since only limited hardness

measurements were taken, this may be an indication of the scatter in hardness values. We have also observed that in this alloy smaller Cr rich precipitates form during ageing. It is possible that these get included in the NiAl volume fraction values from SANS, and in some way contribute to the higher measured strength than expected.

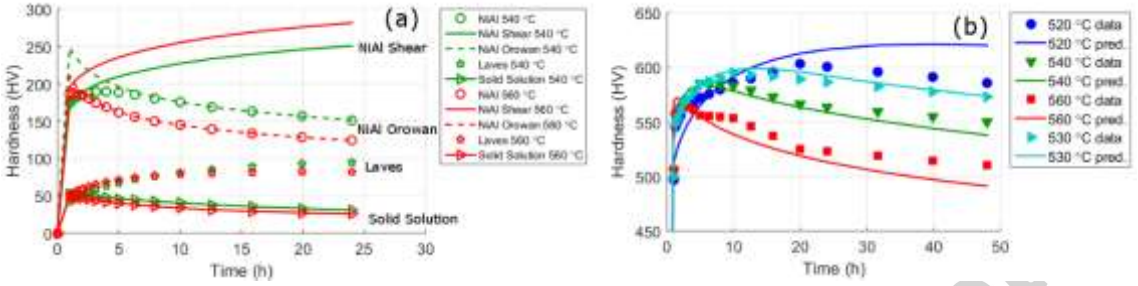

Figure 10, (a) the different predicted strength contributions of 9922, and (b) the total predicted strength at different temperatures.

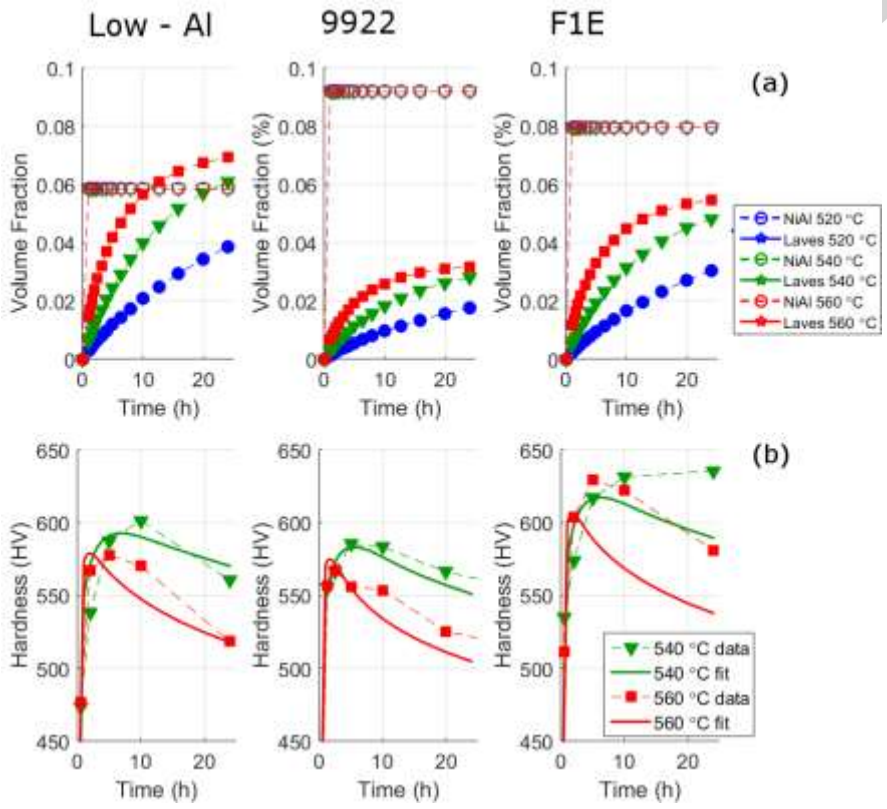

Figure 11, SANS change in the volume fraction of the two precipitates for the three alloys (a). And (b) is the model predictions of strength of the alloys after different ageing times and temperatures, using the SANS results. The model uses the fitting parameters found by only fitting the 9922 data.

6 Conclusions

The evolution and strengthening from nano-sized precipitate are complex problems to understand and model; this is demonstrated by the range of models that have been proposed to explain the behaviour. This work highlights that the combination of small angle neutron scattering (SANS) and atom probe tomography (APT) provide an effective way to provide experimental characterisation to help verify these models. The two methods are complementary, allowing information of changes at the nano-scale of many samples to be determined that is representative of the bulk material. In this work, APT results are used as input for SANS analysis to provide details of: (1) the size distribution of the phases, (2) volume fraction of the phase at one measurement point, (3) composition of phases to calculate volume fraction at other temperature and times. In turn, the SANS analysis has provided details of the change in size, volume fraction and composition of phases during ageing. These SANS results were shown to be consistent with precipitate evolution from: (a) APT results of the alloy, (b) other research on precipitation, (c) and models of precipitate evolution. However, there were some discrepancies; these are thought to be more likely to be due to intrinsic difficulties of the characterisation methods, than indicative of actual differences.

In the final part of this work we considered how the precipitate population influences the strengthening of the alloy. We presented a model which described the different contributions to the strengthening of the alloy. The two precipitates contribute in different ways because of the differences in their evolution. For NiAl, because of their small size and almost constant volume fraction, their strengthening mechanism changes from shear to Orowan looping as they grow. It is this transition that is the cause of the characteristic peak-strength of this alloy. Conversely Laves phase, in the growth stage

throughout, contributes more strength to the alloy with increasing ageing times. Despite its simplicity the model showed good agreement with experimental results.

Acknowledgements

The current research was funded by Innovate UK and Rolls-Royce plc as part of SILOET Project 6 - Core Technology Validation: Systems (reference 110035). The provision of materials and technical support from Rolls-Royce plc is gratefully acknowledged. We would also like to thank Elliott Gilbert and ANSTO beamline for the SANS experiment at the Quokka beamline; and the developers of SasView, http://www.sasview.org/.

REFERENCES

[1] M. Schober, R. Schnitzer, H. Leitner, Precipitation evolution in a Ti-free and Ti-containing stainless maraging steel, Ultramicroscopy. 109 (2009) 553–562. doi:10.1016/j.ultramic.2008.10.016.

[2] S.W. Ooi, P. Hill, M.J. Rawson, H.K.D.H. Bhadeshia, Effect of retained austenite and high temperature Laves phase on the work hardening of an experimental maraging steel, Mater. Sci. Eng. A. 564 (2013) 485–492. doi:10.1016/j.msea.2012.12.016.

[3] J.W. Martin, Precipitation Hardening, in: Second Edi, Butterworth-Heinemann, Oxford, 1998. doi:http://dx.doi.org/10.1016/B978-0-7506-3885-2.50006-2.

[4] E. Orowan, Internal Stress in Metals and alloys, in: Symp. Intern. Stress. Met. Alloy. Inst. Met., London, 1948: p. 451.

[5] Z. Guo, W. Sha, Quantification of Precipitation Hardening and Evolution of Precipitates., Mater. Trans. 43 (2002) 1273–1282. doi:10.2320/matertrans.43.1273.

[6] L.M. Brown, R.K. Ham, Strengthening methods in crystals, Elsevier Publishing Company LTD, Oxford, 1971.

[7] D.H. Bratland, O. Grong, H. Shercliff, O.R. Myhr, S. Tjotta, Overview No. 124: modelling of precipitation reactions in industrial processing, Acta Mater. 45 (1997) 1–22. doi:10.1016/S1359-6454(96)00100-0.

[8] S. Esmaeili, D.J. Lloyd, W.J. Poole, Modeling of precipitation hardening for the naturally aged Al-Mg-Si-Cu alloy AA6111, Acta Mater. 51 (2003) 3467–3481. doi:10.1016/S1359-6454(03)00167-8.

[9] Grong, H.R. Shercliff, Microstructural modelling in metals processing, Prog. Mater. Sci. 47 (2001) 163–282. doi:10.1016/S0079-6425(00)00004-9.

[10] H. Leitner, R. Schnitzer, M. Schober, S. Zinner, Precipitate modification in PH13-8 Mo type maraging steel, Acta Mater. 59 (2011) 5012–5022. doi:10.1016/j.actamat.2011.04.053.

[11] T.L. Martin, A. Radecka, L. Sun, T.H. Simm, D. Dye, K.M. Perkins, B. Gault, M.P. Moody, P.A.J. Bagot, Insights into microstructural interfaces in aerospace alloys characterised by atom probe tomography, Mater. Sci. Technol. 32 (2016) 232–241. doi:10.1179/1743284715Y.0000000132.

[12] L. Sun, T.H. Simm, T.L. Martin, S.W. Ooi, S. McAdam, D. Galvin, K.M. Perkins, H.K.D.H. Bhadeshia, A novel ultra-high strength maraging steel with balanced ductility and creep resistance achieved by nanoscale β-NiAl and Laves phase precipitates, Unpubl. Work. (2017).

[13] D.M. Collins, R.K. Heenan, H.J. Stone, Characterization of Gamma Prime (γ′) Precipitates in a Polycrystalline Nickel-Base Superalloy Using Small-Angle Neutron Scattering, Metall. Mater. Trans. A. 42 (2011) 49–59. doi:10.1007/s11661-010-0466-1.

[14] N.H. Van Dijk, W.G. Bouwman, S.E. Offerman, M.T. Rekveldt, J. Sietsma, S. Van der Zwaag, A. Bodin, R.K. Heenan, High temperature SANS experiments on Nb (C, N) and MnS precipitates in HSLA steel, Metall. Mater. Trans. A. 33 (2002) 1883–1891. doi:10.1007/s11661-002-0021-9.

[15] E.. Shin, B.. Seong, Y.. Han, C.. Lee, H.. Kim, Study of precipitate and texture in low-carbon steels by neutron scattering techniques, Phys. B Condens. Matter. 350 (2004) E475–E478. doi:10.1016/j.physb.2004.03.124.

[16] R. Tewari, S. Mazumder, I.S. Batra, G.K. Dey, S. Banerjee, Precipitation in 18 wt% Ni maraging steel of grade 350, Acta Mater. 48 (2000) 1187–1200. doi:10.1016/S1359-6454(99)00370-5.

[17] T. Dorin, A. Taylor, K. Wood, J. Wang, P.D. Hodgson, N. Stanford, Complex precipitation phenomena in strip cast steels with high sulfur and copper contents, J. Appl. Crystallogr. 49 (2016) 1777–1785. doi:10.1107/S1600576716013054.

[18] T. Dorin, K. Wood, A. Taylor, P. Hodgson, N. Stanford, Quantitative examination of carbide and sulphide precipitates in chemically complex steels processed by direct strip casting, Mater. Charact. 112 (2016) 259–

268. doi:10.1016/j.matchar.2015.12.028.
[19] M. Muthig, Complex SANS / SAXS Data Evaluation , Simulation and Interpretation with Regard to Statistical Inference, Technischen Universtat at Berlin, 2015.
[20] T.L. Martin, A. Radecka, L. Sun, T. Simm, D. Dye, K. Perkins, B. Gault, M.P. Moody, P.A.J. Bagot, Insights into microstructural interfaces in aerospace alloys characterised by atom probe tomography, 0 (2015) 1–10. doi:10.1179/1743284715Y.0000000132.
[21] O.C. Hellman, J.B. Du Rivage, D.N. Seidman, Efficient sampling for three-dimensional atom probe microscopy data, Ultramicroscopy. 95 (2003) 199–205. doi:10.1016/S0304-3991(02)00317-0.
[22] S.M. King, Small Angle Neutron Scattering, Mod. Tech. Polym. Charaterisation. 1999 (1999).
[23] V.F. Sears, Neutron scattering lengths and cross sections, Neutron News. 3 (1992) 26–37. doi:10.1080/10448639208218770.
[24] L.A. Feigin, D.I. Svergun, Structure analysis by small-angle X-ray and neutron scattering.pdf, (1987) 335. doi:10.1002/actp.1989.010400317.
[25] A. Guinier, G. Fournet, Small-angle scattering of X-rays, Wiley, 1955.
[26] D. Porter, K. Easterling, Phase transformations in metals and alloys, Zhurnal Eksp. I Teor. Fiz. (1992) 111.
[27] A.P. Li, X., Miodownik, N. Saunders, Modelling of materials properties in duplex stainless steels, Mater. Sci. Technol. 18 (2002) 861–868. doi:10.1179/026708302225004694.
[28] V. Seetharaman, M. Sundararaman, R. Krishnan, Precipitation hardening in a PH 13-8 Mo stainless steel, Mater. Sci. Eng. 47 (1981) 1–11. doi:10.1016/0025-5416(81)90034-3.
[29] P. Liu, A.H. Stigenberg, J.-O. Nilsson, Quasicrystalline and crystalline precipitation during isothermal tempering in a 12Cr-9Ni-4Mo maraging stainless steel, Acta Metall. Mater. 43 (1995) 2881–2890. doi:10.1016/0956-7151(94)00461-P.
[30] G. Ghosh, G.B. Olson, Simulation of paraequilibrium growth in multicomponent systems, Metall. Mater. Trans. A. 32 (2001) 455–467. doi:10.1007/s11661-001-0062-5.
[31] Z. Guo, W. Sha, D. Vaumousse, Microstructural evolution in a PH13-8 stainless steel after ageing, Acta Mater. 51 (2003) 101–116. doi:10.1016/S1359-6454(02)00353-1.
[32] D.H. Ping, M. Ohnuma, Y. Hirakawa, Y. Kadoya, K. Hono, Microstructural evolution in 13Cr–8Ni–2.5Mo–2Al martensitic precipitation-hardened stainless steel, Mater. Sci. Eng. A. 394 (2005) 285–295. doi:10.1016/j.msea.2004.12.002.
[33] G. Dimmler, P. Weinert, E. Kozeschnik, H. Cerjak, Quantification of the Laves phase in advanced 9-12% Cr steels using a standard SEM, Mater. Charact. 51 (2003) 341–352. doi:10.1016/j.matchar.2004.02.003.
[34] P. Hu, W. Yan, W. Sha, W. Wang, Z. li Guo, Y. yin Shan, K. Yang, Study on Laves phase in an advanced heat-resistant steel, Front. Mater. Sci. China. 3 (2009) 434–441. doi:10.1007/s11706-009-0063-7.
[35] P.G. Shewmon, Diffusion in Solids, McGraw-Hill, New York, 1964.
[36] J.W. Christian, The theory of transformations in metals and alloys, Newnes, 2002.
[37] Z. Guo, W. Sha, Quantification of precipitation kinetics and age hardening of Fe–1 2Ni–6Mn alloy during overaging, Mater. Sci. Technol. 18 (2002) 377–382. doi:10.1179/026708302225001732.
[38] C. Stocker, Auswirkungen der Ausscheidungskinetik auf das Kriechverhalten Mo- und B-legierter 9% Cr-Stähle., TU Vienna, 2002.
[39] C. Zener, Theory of Growth of Spherical Precipitates from Solid Solution, J. Appl. Phys. 20 (1949) 950. doi:10.1063/1.1698258.
[40] J.W. Martin, J.W. Martin, R.D. Doherty, B. Cantor, Stability of Microstructure in Metallic Systems, Cambridge University Press, 1997.
[41] T. Gladman, Precipitation hardening in metals, Mater. Sci. Technol. 15 (1999) 30–36. doi:10.1179/026708399773002782.
[42] A. Melander, P.Å. Persson, The strength of a precipitation hardened AlZnMg alloy, Acta Metall. 26 (1978) 267–278. doi:10.1016/0001-6160(78)90127-X.
[43] I.O. Smith, M.G. White, The Origin of the Shear Stress Increment in Aged Ferritic Fe-Ni-Ti-Al Alloys, Metall. Trans. A. 7 (1976) 293–298. doi:10.1007/BF02644470.
[44] Z.K. Teng, G. Ghosh, M.K. Miller, S. Huang, B. Clausen, D.W. Brown, P.K. Liaw, Neutron-diffraction study and modeling of the lattice parameters of a NiAl-precipitate-strengthened Fe-based alloy, Acta Mater. 60 (2012) 5362–5369. doi:10.1016/j.actamat.2012.05.033.
[45] R.E. Smallman, R.J. Bishop, Modern Physical Metallurgy and Materials Engineering, Management. (1999) 368. doi:10.1016/B978-075064564-5/50002-1.
[46] E. Nembach, Particle strengthening of metals and alloys, J. Wiley, 1997.
[47] K. Liu, Y. Shan, Z. Yang, J. Liang, Effect of aging on microstructure and mechanical property of 1900 MPa grade maraging stainless steel, J. Mater. Sci. Technol. 23 (2007) 312–318.
[48] R. Schnitzer, S. Zinner, H. Leitner, Modeling of the yield strength of a stainless maraging steel, Scr. Mater. 62 (2010) 286–289. doi:10.1016/j.scriptamat.2009.11.020.
[49] G.. Ansell, F.. Lenel, Criteria for yielding of dispersion-strengthened alloys, Acta Metall. 8 (1960) 612–616. doi:10.1016/0001-6160(60)90015-8.
[50] T. Narita, S. Ukai, S. Ohtsuka, M. Inoue, Effect of tungsten addition on microstructure and high temperature strength of 9CrODS ferritic steel, J. Nucl. Mater. 417 (2011) 158–161. doi:10.1016/j.jnucmat.2011.01.060.
[51] T. Gladman, The Physical Metallurgy of Microalloyed Steel, The Institute of Materials, London, 1997.

[52] W.C. Leslie, Iron and its dilute substitutional solid solutions, Metall. Trans. 3 (1972) 5–26. doi:10.1007/BF02680580.
[53] H. Sieurin, J. Zander, R. Sandström, Modelling solid solution hardening in stainless steels, Mater. Sci. Eng. A. 415 (2006) 66–71. doi:10.1016/j.msea.2005.09.031.